

Dynamics of Hydrogen-Oxygen-Argon Cellular Detonations with a Constant Mean Mass Divergence

Q. Xiao^{a,*}, M. I. Radulescu^a

^a*Department of Mechanical Engineering, University of Ottawa, Ottawa,
Ontario K1N 6N5, Canada*

Abstract

The present work revisits the problem of modelling the real gaseous detonation dynamics at the macro-scale by simple steady one-dimensional (1D) models. Experiments of detonations propagating in channels with exponentially expanding cross-sections (exponential horns) were conducted in the H₂/O₂/Ar reactive system. Steady detonation waves were obtained at the macro-scale, with cellular structures characterized by reactive transverse waves. For all the mixtures studied, the dependence of the mean detonation speed was found to be in excellent agreement with first principles predictions of quasi-1D detonation dynamics with lateral mass divergence predicted from detailed chemical kinetic models. This excellent agreement departs from the earlier experiments of Radulescu and Borzou (2018) in more unstable detonations. The excellent agreement is likely due to the much longer reaction zone lengths of diluted hydrogen oxygen detonations at low pressures, as compared with the characteristic induction zone lengths. While the cellular instability modifies the detonation structures induction zone, the detonation dynamics at the macro-scale are arguably controlled by its hydrodynamic thickness. Near the limit, minor discrepancy is observed, with the experimental detonations typically continuing to propagate to slightly higher lateral strain rates and higher velocity deficits.

Keywords: H₂/O₂/Ar, mass divergence, cellular detonation dynamics, steady model

1. Introduction

Real detonations in gases have been experimentally observed to travel at a speed smaller than the ideal Chapman-Jouguet (CJ) detonation speed by a velocity deficit, due to the presence of non-ideal effects [1, 2]. These non-ideal factors include lateral mass divergence, unsteadiness, and momentum and heat losses [1]. Extensive efforts have been made to quantitatively compare the experimentally measured velocity deficits and propagation limits with the theoretical predictions made by relatively simple models, which build up on the classical one-dimensional (1D) Zeldovich-von Neumann-Doering (ZND) model [3–16]. The multi-dimensional transient cellular structures, consisting of an intricate ensemble of interacting triple points, shear layers, and transverse waves, of the real gaseous detonations, however, greatly complicate these attempts.

*Corresponding author:
Email address: qxiao067@uottawa.ca (Q. Xiao)

They give rise to substantial deviations from the classical 1D ZND detonation structures [2, 17]. A significant question hence comes up that, can the extended ZND model, which neglects the time varying cellular structures, be able to model the real detonation dynamics in the presence of losses at the macro-scale? The present paper addresses this question.

This question has also been attempted in the past by investigating detonation propagation in narrow tubes [8, 9, 11–15] and tubes with porous walls [18, 19]. The mean propagation velocities of detonations under varied initial pressures as well as the propagation limits were experimentally determined for various mixtures. Due to the lateral mass divergence from the growth of the viscous boundary layer on tube walls acting as a mass sink [4] or from the porosity of the walls, streamlines in the steady reaction zone are diverged resulting in a globally curved detonation front experiencing a velocity deficit [20]. In narrow tubes, the boundary layer theory of Fay [4] was adopted for evaluating the global lateral mass divergence; while in porous tubes, where constant mass divergence was assumed, it was estimated from the permeability of the porous wall by assuming a choked flow. The generalized ZND model with lateral mass divergence was then applied to model the detonation dynamics. The authors have found that, the experimentally obtained detonation velocity deficits and propagation limits are in generally good agreement with the theoretical predictions, made with the steady ZND model for weakly unstable detonations, which are characterized by regular cellular structures; while for the unstable detonations with irregular cells, the agreement is poor. Nevertheless, a number of simplifying assumptions and matching constants were made in these works for the predictions. Firstly, there exist limitations in the unrealistic assumption of uniform mass divergence, i.e., uniform curvature, for detonations in narrow and porous tubes, as Chinnayya et al. [20] and Mazaheri et al. [21] have numerically demonstrated that a curved detonation front with mass divergence due to wall boundary layers or permeability is not expected to have a unique curvature. Moreover, Fay-type models [8, 12–15] require the empirical inputs of a specifically defined value of pressure ratio ϵ , and a particular length scale for modelling the flow divergence rate, whose impact on the predictions has not been evaluated. All these factors thus potentially diminish the values of the comparisons in relevant works.

Very recently, Radulescu and Borzou [22] experimentally formulated a novel solution allowing for making a meaningful comparison of the experimental results with theoretical models. Their experimental technique involved two exponentially shaped channels (exponential horns). The constant logarithmic derivative of the cross-sectional area enabled detonations to propagate with a constant mean mass divergence in quasi-steady state. Two mixtures of different regularity were tested, i.e., the highly unstable one of $\text{C}_3\text{H}_8/5\text{O}_2$ and weakly unstable one of $2\text{C}_2\text{H}_2/5\text{O}_2/21\text{Ar}$. Firstly, they showed that detonations in the exponential horns propagated at a constant average speed, which was controlled by the magnitude of the lateral mass divergence. Beyond a critical value of mass divergence, detonations were not possible. Moreover, they compared the experimentally obtained relationship, between the detonation velocity deficit and its front's global curvature, with the generalized ZND model in the presence of lateral mass divergence. The predictions made with the steady ZND model for the velocity deficit disagreed with the experiments. The weakly unstable $2\text{C}_2\text{H}_2/5\text{O}_2/21\text{Ar}$ detonations showed better agreement, between experiments and the theoretical predictions, than that of the highly unstable $\text{C}_3\text{H}_8/5\text{O}_2$ detonations. An interesting question then arises that, can the extended ZND model better predict detonation dynamics of much less unstable mixtures, in spite of the cellular structures? This becomes the objective of the present work.

It is well known that argon diluted $2\text{H}_2/\text{O}_2$ detonations have the weakest instability among those typically investigated experimentally [17, 19] and have a very regular cellular structure.

The chemical kinetics of H₂ decomposition is also better known than for hydrocarbon. Therefore, the present study aims to extend the above well-posed technique to more stable mixtures of 2H₂/O₂/2.0Ar, 3.0Ar, 4.5Ar, and 7.0Ar, for the purpose of investigating in detail the dynamics of very regular cellular detonations in exponentially diverging channels. It eventually permits a conclusive answer for the predictability of detonation dynamics by the generalized ZND model with lateral mass divergence.

2. Experimental Details

The experiments were conducted in a 3.4-m-long aluminium rectangular channel with an internal height and width of 203 mm and 19 mm, respectively. A sketch of the experimental set-up is shown in Fig.1, which is the same as that adopted by Radulescu and Borzou [22]. The shock tube comprises three sections, a detonation initiation section, a propagation section, and a test section. The mixture was ignited in the first section by a high voltage igniter (HVI), which could store up to 1000 J with the deposition time of 2 μ s. Mesh wires were inserted in the initiation section for promoting the formation of detonations. Eight high frequency piezoelectric PCB pressure sensors (p1-p8) were mounted flush on the top wall of the shock tube to record pressure signals and then obtain the propagation speeds by using the time-of-arrival method. The test section was equipped with two glass panels in order to visualize the detonation evolution process. For the safety purpose of performing experiments at high initial pressures, the visualization glass panels were alternatively replaced by aluminum ones.

Two different polyvinyl-chloride (PVC) ramps, which enabled the cross-sectional area $A(x)$ of the channel to diverge exponentially with a constant logarithmic area divergence rate ($K = \frac{d(\ln A(x))}{dx}$), were adopted in the test section. Dimensions of the ramps are shown in Fig.1(b). The large ramp had the logarithmic area divergence rate of 2.17 m⁻¹, while for the small one such rate was 4.34 m⁻¹. At the entrance, a protruded rounded tip was kept for minimizing the effects of shock reflection on the detonation front. The initial gap between the ramp tip and the top wall of the channel is 23 mm in height. The height between the exponentially curved wall and the top wall is given by $y_{wall} = y_0 e^{Kx}$ for $x > 0$ and by $y_{wall} = y_0$ otherwise.

The mixtures presently studied were stoichiometric hydrogen/oxygen with different argon dilution, i.e., 2H₂/O₂/2.0Ar, 3.0Ar, 4.5Ar, and 7.0Ar. Each of them was prepared in a separate mixing tank by the method of partial pressures and was then left to mix for more than 24 hours. The mixture was introduced into the shock tube through both ends of the tube at the desired initial pressure with an accuracy of 70 Pa. Before filling with the test mixture in every single experiment, the shock tube was evacuated below the absolute pressure of 90 Pa. A driver gas of C₂H₂/3O₂ separated by a diaphragm, as shown in Fig.1(a), was used in the initiation section for low initial pressures, under which detonations of the test gas can not be initiated successfully before entering the test section. For visualizing the detonation evolution process along the exponential ramp, a large-scale shadowgraph system was adopted by using a 2m×2m retro-reflective screen with an incandescent filament light source of 1600 W Xenon arc lamp from Newport. The resolution of the high-speed camera was 1152×256 px² with the frame rate of 42049 fps or 42496 fps. The exposure time was set to 2.0 μ s. Alternatively, a Z-type schlieren setup [23] with a vertical knife edge was also utilized with a light source of 360 W. The resolution of the high-speed camera was 384×288 px² with the framing rate of 77481 fps and the exposure time of 0.468 μ s. Note that the background of each shadowgraph and schlieren photograph in the present study was appropriately removed and the images were postprocessed.

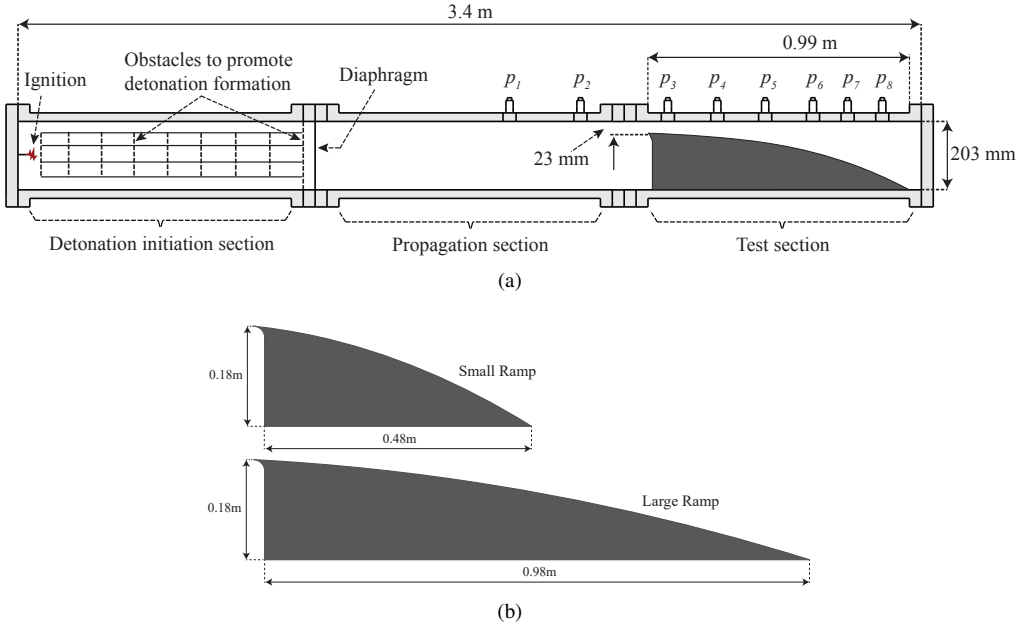


Figure 1: Experimental set-up for diverging detonation experiments: (a) the shock tube with the large ramp inserted in the test section and (b) the exponentially diverging ramps.

3. Experimental Results

3.1. Propagation of $2\text{H}_2/\text{O}_2/2\text{Ar}$ detonations along the large ramp

The superimposed shadowgraph photos illustrating the evolution of diverging detonation fronts along the large ramp for the mixture of $2\text{H}_2/\text{O}_2/2\text{Ar}$, at an initial pressure of 14.8 kPa and 12.4 kPa, respectively, are shown in Fig.2. The detonation propagated from left towards right. The detonation front acquired a large number of small-sized cellular structures, and was noticeably curved with a characteristic curvature due to the cross-sectional area divergence. Within the limited resolution of the photographs, transverse waves can be recognized starting from triple points and extending backward downstream. One can also note that, as the cross section area of the channel increases, new transverse waves were continuously generated and the average transverse wave spacing appeared to remain constant. This suggests that the cell size remains constant in the self-sustained propagation of diverging detonations along the ramp. The average detonation cell size measured in Fig.2(a) and (b) is approximately 17.0 mm and 21.0 mm, respectively, which are found to be larger than the values of 10.5 mm and 13.5 mm obtained from the Detonation Database [24] for the same initial pressures.

On the other hand, the theoretically expected arcs of the curvature from the quasi-1D approximation, whose radius equals the reciprocal of the logarithmic area divergence rate $K = 2.17\text{m}^{-1}$, were obtained and compared with the real detonation fronts in experiments. These arcs of circles with the radius of $1/K = 0.46\text{m}$ are denoted by the dashed red lines in Fig.2. The comparison shows that the detonation front's global curvature is in very good agreement with that expected by the quasi-1D approximation for designing the exponential geometry, despite some minor deviations near the end of the ramp. These small deviations, as a result of the error in the quasi-1D

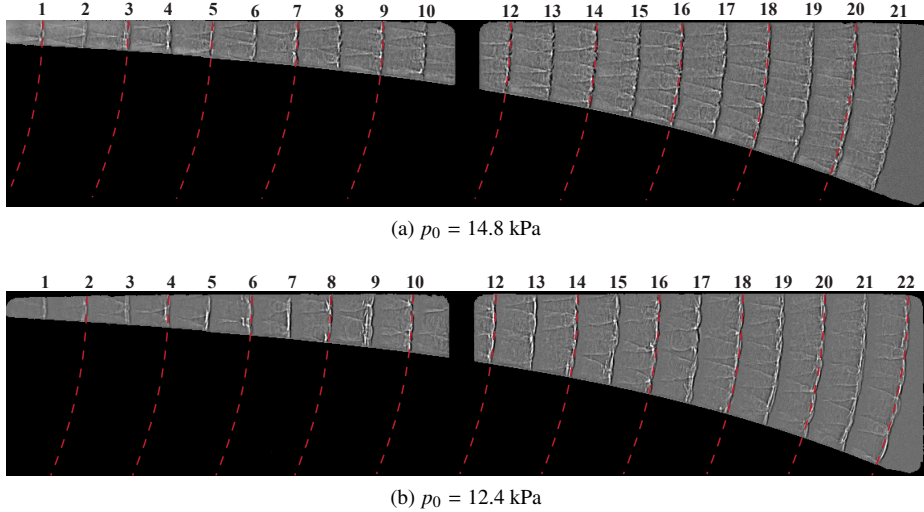


Figure 2: The superposition of detonation fronts along the large ramp at different instants for the mixture of $2\text{H}_2/\text{O}_2/2\text{Ar}$; red lines denote arcs of circles with the expected curvature from the quasi-1D approximation.

approximation, have been quantitatively estimated by Radulescu and Borzou [22]. It thus indicates the appropriateness of assuming steadily travelling detonations with a constant global curvature, i.e., constant mean mass divergence, inside the exponential horn, which was also numerically demonstrated by Radulescu and Borzou [22].

The detonation propagation process for other lower initial pressures, near the limit, is illustrated in the superimposed shadowgraph photos of Fig.3. With the decrease of the initial pressure for reducing the kinetic sensitivity of mixtures, detonation cells are considerably enlarged. The classical triple-shock structure, comprising a Mach stem, an incident shock, and a transverse wave that extends behind the detonation front, can now be clearly observed. One can also observe the consumption of the unreacted induction zones behind the incident shock by the passage of transverse waves, e.g., see Frame 15 through Frame 18 in Fig.3(a), implying the reactivity of these waves. This type of reactive transverse wave has been investigated first in detail by Subbotin [25] for the marginal, weakly unstable detonations and subsequently reported in a series of numerical and experimental works, e.g., Sharpe [26], Pintgen et al. [27], and Austin [28]. When the initial pressure was further decreased to approach the failure conditions, below which detonations are not possible, the reaction zone structure was excellently visualized (Fig.3(b)-(d)). These near-limit detonations were able to travel successfully with only one reactive transverse wave, which is interpreted as a transverse detonation [29], as can be easily seen from Fig.3(b)-(d). When delineating the track of the triple point, one can readily obtain the single-headed detonation cell, denoted by the red dashed line in Fig.3(b)-(d). Clearly, as the detonation propagated towards the end, the detonation cell size considerably increased. An alternative explanation of the enlarging cells, in spite of the constant mean propagation speed, is the stabilization mechanism proposed by Short et al. [30]. Clearly in these curved detonations, the growth of the detonation front's area may be higher than the intrinsic transverse instability growth rate, thus resulting in the single-headed detonation of continuously increasing cell size without birth of any new transverse waves.

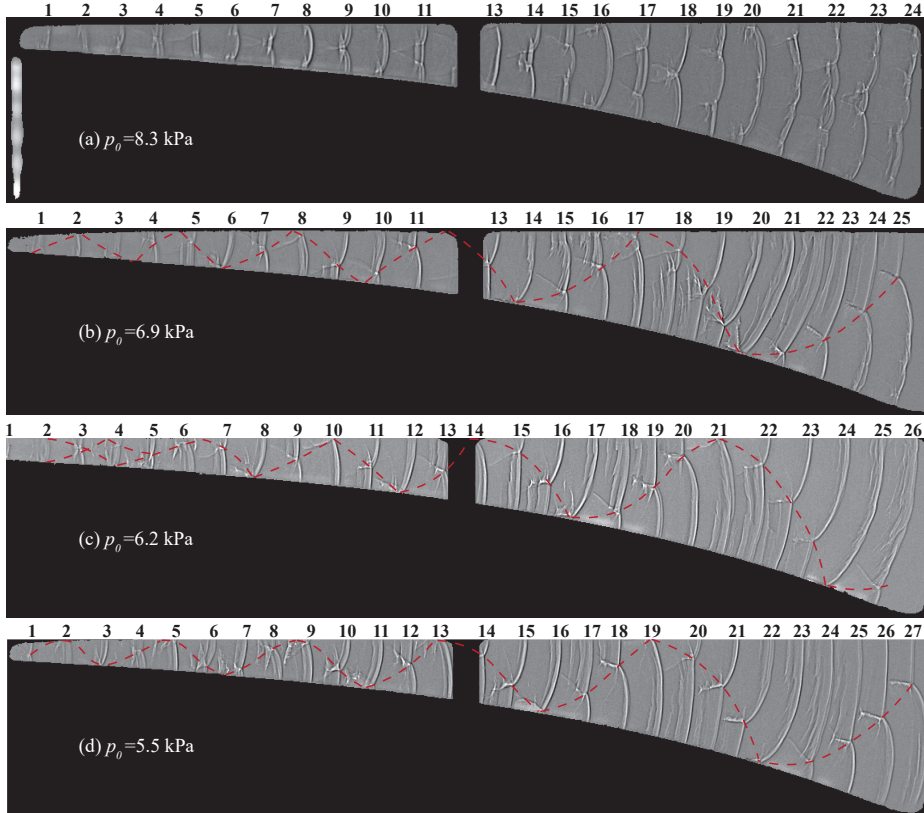


Figure 3: The evolution of $2\text{H}_2/\text{O}_2/2\text{Ar}$ detonation fronts along the large ramp under different initial pressures near the propagation limit.

Figure 4 shows the detailed structure of the characteristic transverse detonation. It is qualitatively similar to that documented by Gamezo et al. [29]. It consists of two parts, a reactive one connected to the triple point and the other non-reactive one that extends far behind. The reactive part, i.e., transverse detonation, propagates transversely along the large induction zone and is strong enough to burn almost all the material except for a thin tail in the vicinity of the triple point [29]. The generation mechanism of this thin non-reactive tail in the gap between the leading shock and the transverse detonation front has been clarified by Gamezo et al. [29] due to the low temperature of the mixture in an embedded double Mach reflection. The transverse detonation, providing energy release via consuming the unburned fuels behind the leading shock, thus constitutes a possible mechanism for promoting the near-limit single-headed detonation propagation.

Quantitatively, profiles of the locally averaged speed both along the top and bottom curved walls are shown in Fig.5, corresponding to the detonation evolution in Fig.3. The speed was normalized by the ideal CJ detonation speed calculated with the NASA chemical equilibrium code CEA [31]. The first observation from Fig.5 is that the local speed profiles exhibit periodic fluctuations, ranging from the maximum of $\sim 1.2 D_{\text{CJ}}$ to the minimum of $\sim 0.5 D_{\text{CJ}}$. These characteristic fluctuations very well illustrate the cyclic dynamics of detonations propagating in

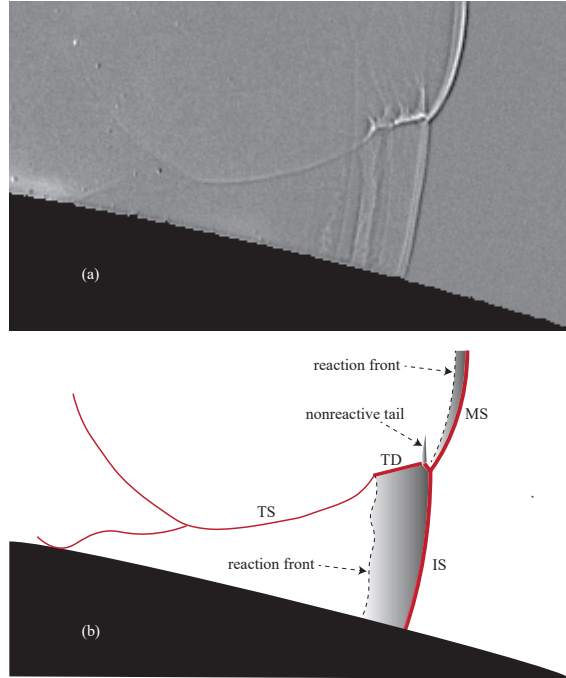


Figure 4: Details of the characteristic transverse detonation: (a) zoom-in of the cellular structure of Frame 21 in Fig.3(d), and (b) sketch of the main features. MS: Mach Stem, IS: Incident Shock, TD: Transverse Detonation, TS: Transverse Shock. Note that the shaded zone between the reaction front and the detonation front is the unburned induction zone.

cells. As the detonation propagated to the right end, the fluctuation period increased, implying an increasing length scale of the detonation cell. This is consistent with the finding from Fig.3 that the detonation cell size increased as a result of the diverging area for the near-limit detonations. Secondly, the local speeds along the top and bottom curved walls follow the same evolution behaviors, and the difference between their global mean propagation speeds, denoted by the dashed lines, is very limited (within 3% of D_{CJ}). Moreover, despite the significant variations of local speeds periodically, detonations in each cellular cycle appeared to propagate at the same constant mean speed, i.e., the global mean propagation speed. It thus suggests the appropriateness of applying the quasi-steady assumption to near-limit detonations inside the exponential horn.

For the critical pressure of 5.5 kPa, below which detonations were unable to propagate, six experiments in total were repeated. It was found that three of them could have successfully propagating single-headed detonations while the rest three finally failed. Understandably, for the very limit pressure, whether detonation survives or fails depends on probability due to its inherently stochastic property. For example, studies on detonation diffraction [32, 33] have also similarly reported the Go/No-Go phenomenon for detonations diffracting under critical pressures. Any slightly different perturbations during the whole evolution process can sensitively impact the result of Go or No-Go for detonation propagation in the critical pressure range. Figure 6 shows the failing process of the critical detonation and correspondingly its top-wall speed profile. Before the failure, it was similar to that of the successful cases in the propagation mechanism of a single-headed detonation. As the detonation proceeded, the trailing reaction front was gradually

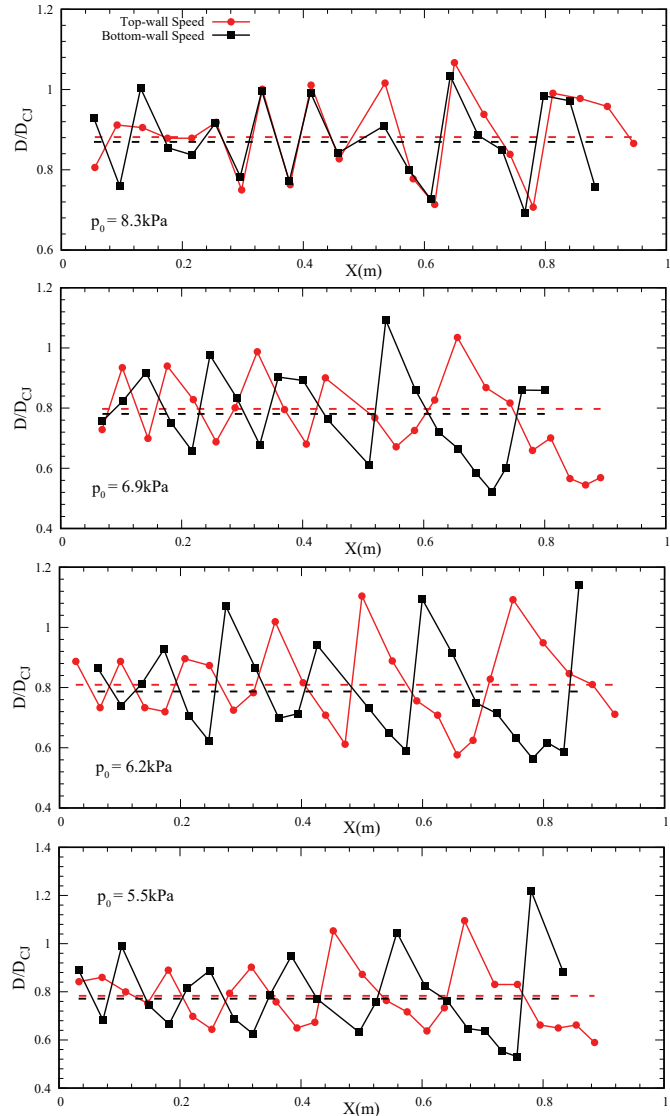


Figure 5: Local speed profiles (along the top and bottom curved walls) for $2\text{H}_2/\text{O}_2/2\text{Ar}$ detonations in Fig.3 for different initial pressures. The dashed lines represent the global mean propagation speed.

detached from the leading shock and unreacted tongues were formed behind, with the transverse wave becoming inert. Finally, the detonation failed with the complete detachment of the reaction front from the leading shock (see Frame 28 in Fig.6(a)), thereby resulting in the continuous decay of the shock, which can be seen from the continuously decreasing speed in Fig.6(b). Of noteworthy is that no distinctive transverse detonations were observed in the decoupled shock-flame complex for the failure case.

In addition, the average detonation cell size was also obtained from the shadowgraph photos

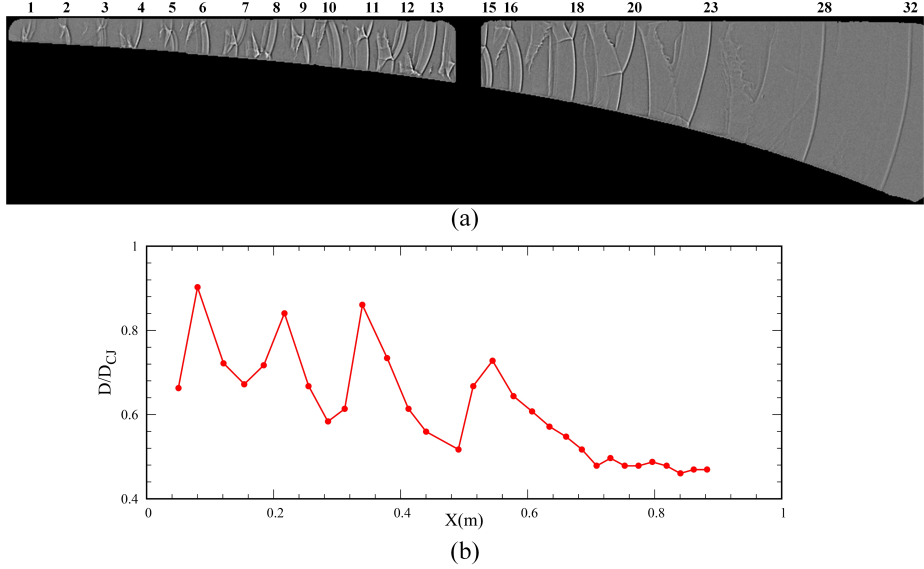


Figure 6: Shadowgraph photos (a) and top-wall speed profiles (b) of a failed detonation at the initial pressure of 5.5 kPa for the mixture of $2\text{H}_2/\text{O}_2/2\text{Ar}$.

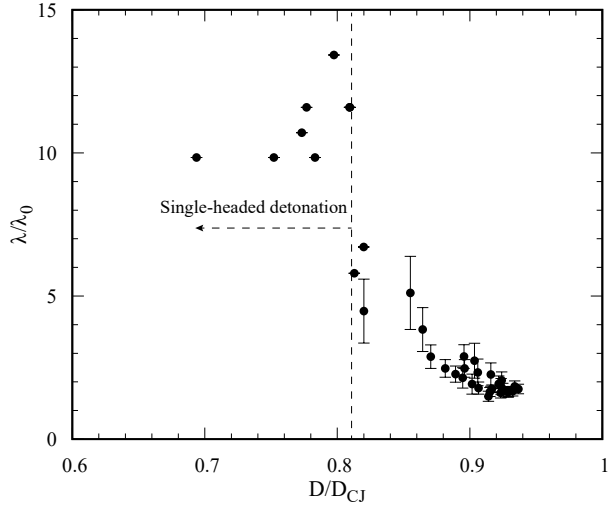


Figure 7: The ratio of estimated cell size (λ) in the present large ramp experiments to previously reported cell size (λ_0) as a function of the normalized mean propagation speed D/D_{CJ} for detonations in the mixture of $2\text{H}_2/\text{O}_2/2\text{Ar}$.

of each experiment, as illustrated in Fig.7 characterizing the relationship between the ratio of the presently estimated cell size (λ) to previously reported cell size (λ_0) [34, 35], and the mean propagation speed, normalized by the ideal CJ value. Note that the relation of λ_0 was given by $\lambda_0(p) = 443.3p^{-1.39}$, which was fitted from the data in the Detonation Database [24]. Also, it is reasonable to assume these reported cell sizes for detonations with very limited or no ve-

locity deficits, i.e., ideal CJ detonations. The results from Fig.7 show that the normalized cell size (λ/λ_0) increased considerably when decreasing the mean propagation speed with respect to the ideal CJ speed (D/D_{CJ}), suggesting a strong dependence of the cell size on the detonation velocity deficit. When the mean propagation speed further decreased to $\sim 0.8D_{CJ}$, detonations started to be organized in a single-headed one, whose cell size was about 10~15 times larger than that of the ideal CJ detonation at the same initial pressure. Previous works proposed the onset of single-headed spinning detonations as a criterion for propagation limits of detonations in narrow tubes [36, 37]. Here, it further demonstrates the characterization of propagaton limits inside the exponentially diverging channel by a single-headed detonation, organized with a distinctive transverse detonation.

3.2. Propagation of $2\text{H}_2/\text{O}_2/2\text{Ar}$ detonations along the small ramp

In this part, experiments were performed for detonations propagating along the small ramp of a higher area divergence rate of $K = 4.34\text{m}^{-1}$, i.e., double that of the large ramp. Visualization of the reaction zone structures of detonations under varied initial pressures near the limit, as shown in Fig.8, enables us to make the following observations. At 10.3 kPa, detonations propagated with two triple points, i.e., one pair of transverse waves, along the detonation front ((Fig.8(a))). Evidently, these transverse shocks were reactive in burning the unburned gases behind the leading shock, preventing the generation of significant unreacted gas pockets [27, 28]. When the

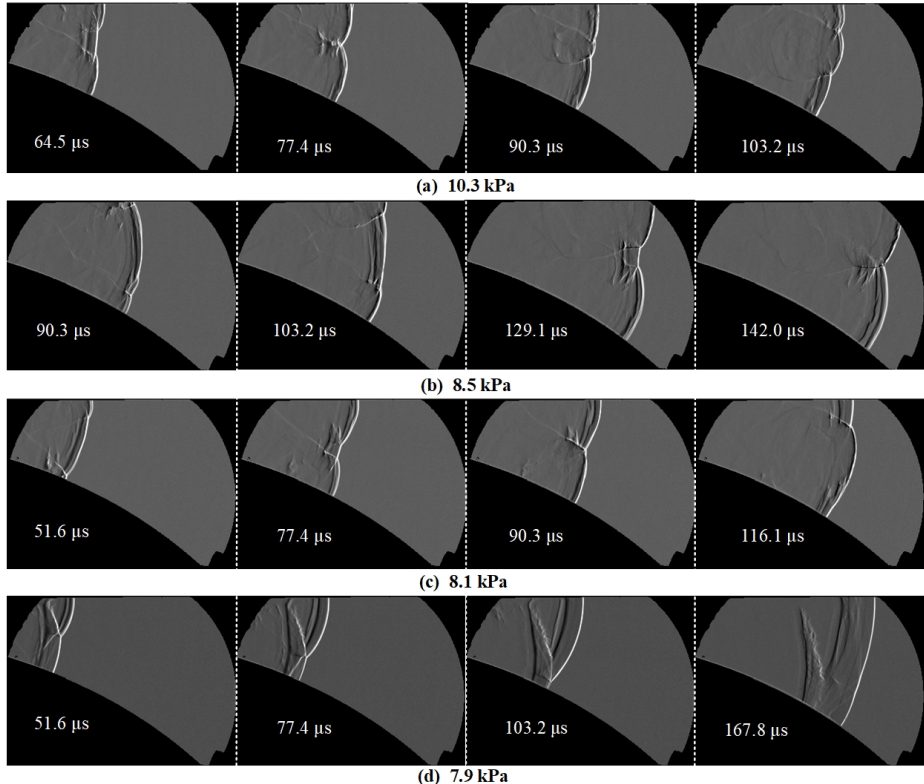


Figure 8: Schlieren photographs of near-limit detonations along the small ramp for the mixture of $2\text{H}_2/\text{O}_2/2\text{Ar}$.

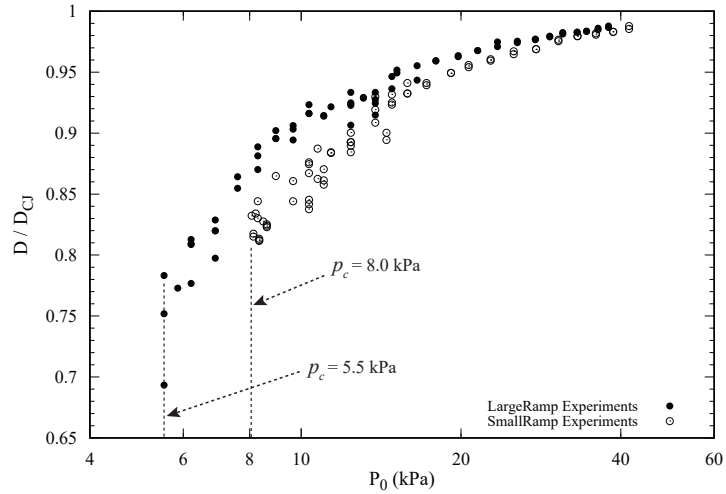


Figure 9: Average speeds normalized by the corresponding CJ speeds with respect to different initial pressures for the mixture of $2\text{H}_2/\text{O}_2/2.0\text{Ar}$.

initial pressure was decreased to approach the critical one of 8.1 kPa, a single-headed detonation featuring a transverse detonation was formed, as is clearly illustrated in Fig.8(b) and (c). Below this critical pressure, the leading shock was found to continuously detach from the trailing reaction front with the transverse wave being inert, which can be seen from Fig.8(d). Since the average speeds along the walls were measured to be only 0.5~0.6 D_{CJ} , detonations can thus be interpreted as finally failed at the initial pressure of 7.9 kPa in Fig.8(d). It is not clear if such case in a much longer horn would have been possible.

The global mean propagation speeds of the $2\text{H}_2/\text{O}_2/2\text{Ar}$ detonations, measured in all the experiments of both ramps, are shown in Fig.9 as a function of initial pressures. As a result of the mass divergence, experienced by detonations inside the cross-section area diverging channels, the mean propagation speed is smaller than its ideal CJ detonation speed by a velocity deficit. These velocity deficits increase with the rate of mass divergence, as can be easily concluded in Fig.9 from the higher propagation speeds measured in the large ramp experiments ($K = 2.17\text{m}^{-1}$) than that of the small ramp ($K = 4.34\text{m}^{-1}$) under the same initial pressures. As the initial pressure is reduced, the deviation of the mean propagation speed from the ideal CJ value becomes larger, implying a more significant role of mass divergence in impacting detonations of lower initial pressures. Near the limit, such velocity deficits can reach 20% ~ 30% of the CJ value. One more observation is the higher propagation limit p_c of detonations along the small ramp. This can be interpreted as the consequence of more losses experienced by detonations along the small ramp due to its larger mass divergence rate, thus giving rise to a higher critical pressure.

3.3. Detonation behaviors with different argon dilutions

In the present study, experiments of detonations in stoichiometric H_2/O_2 mixtures with other argon dilutions both along the large ramp and small ramp were also performed. It served the purpose of both qualitatively and quantitatively demonstrating the influence of argon dilution on detonation behaviors. The mixtures involved in this part are $2\text{H}_2/\text{O}_2/3.0\text{Ar}$, 4.5Ar, and 7.0Ar, corresponding to the argon dilution of 50%, 60%, and 70%, respectively. Figure 10 shows the superimposed schlieren photographs illustrating the evolution of detonations, well above the limit,

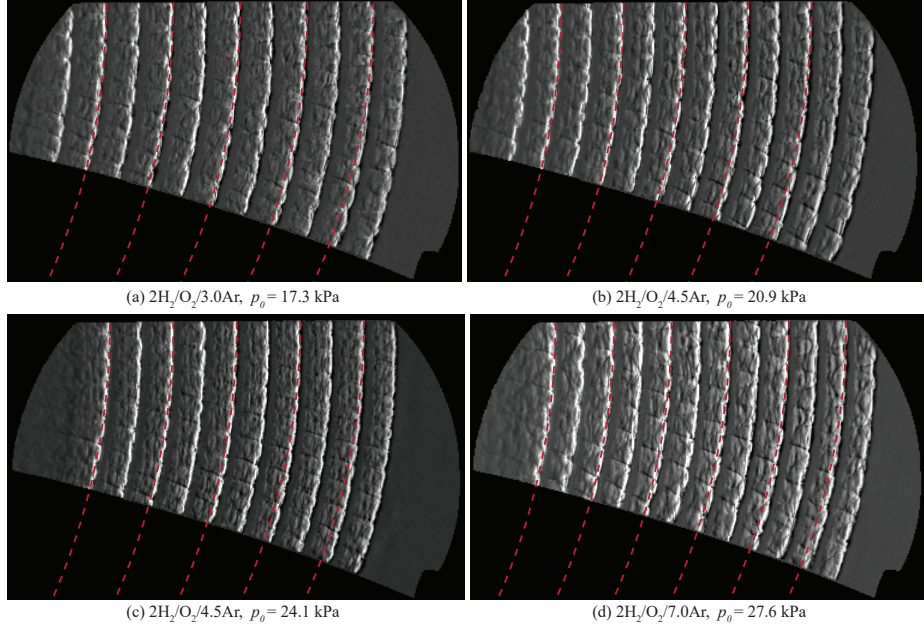


Figure 10: Comparison of the superimposed detonation fronts near the end of the large ramp with the curvature (denoted by red lines) expected from the quasi-1D approximation for different mixtures.

along the large ramp for different mixtures. The curved detonation fronts were uniformly textured with triple points, with transverse waves extending downstream behind the leading shock. Again, cell sizes can be reasonably assumed to remain constant for detonations inside the exponential horn, under initial pressures far away from the limit. Moreover, comparisons of these experimentally obtained detonation fronts with arcs of the expected curvature from the quasi-1D approximation were made. The very good agreement between the real curved detonation fronts and the theoretically expected arcs, denoted by the red dashed lines in Fig.10, demonstrates the independence of the detonation front's global curvature on mixture compositions and initial pressures. It is thus indicative of the fact that argon diluted H_2/O_2 detonations, well above the limit, propagate in quasi-steady state at the macro-scale with the same constant global curvature, i.e., constant mean mass divergence.

The visualized cellular structures of near-limit detonations in mixtures of $2\text{H}_2/\text{O}_2/3.0\text{Ar}$, 4.5Ar , and 7.0Ar show qualitatively the same behaviors as that of $2\text{H}_2/\text{O}_2/2.0\text{Ar}$ detonations. For example, Fig.11 gives the evolution process of detonations with one pair of classical triple-shock structures in the mixture of $2\text{H}_2/\text{O}_2/4.5\text{Ar}$ at the initial pressure of 11.2 kPa. It excellently demonstrates the interactions between the very regular cellular structures, including the collision of transverse waves and their reflections from the walls. Due to the reactive portion of the transverse shock, sweeping across the unburned induction zone behind the incident shock, no significant unreacted gas pockets were observed. The detailed propagation process of single-headed detonations is illustrated in Fig.12 for the mixture of $2\text{H}_2/\text{O}_2/3.0\text{Ar}$. Prior to the formation of a transverse detonation, some unburned gases can be observed behind the transverse wave in the first three frames, implying that this transverse shock was non-reactive and of weak type. The transverse detonation occurred after the reflection of the inert transverse wave from the curved

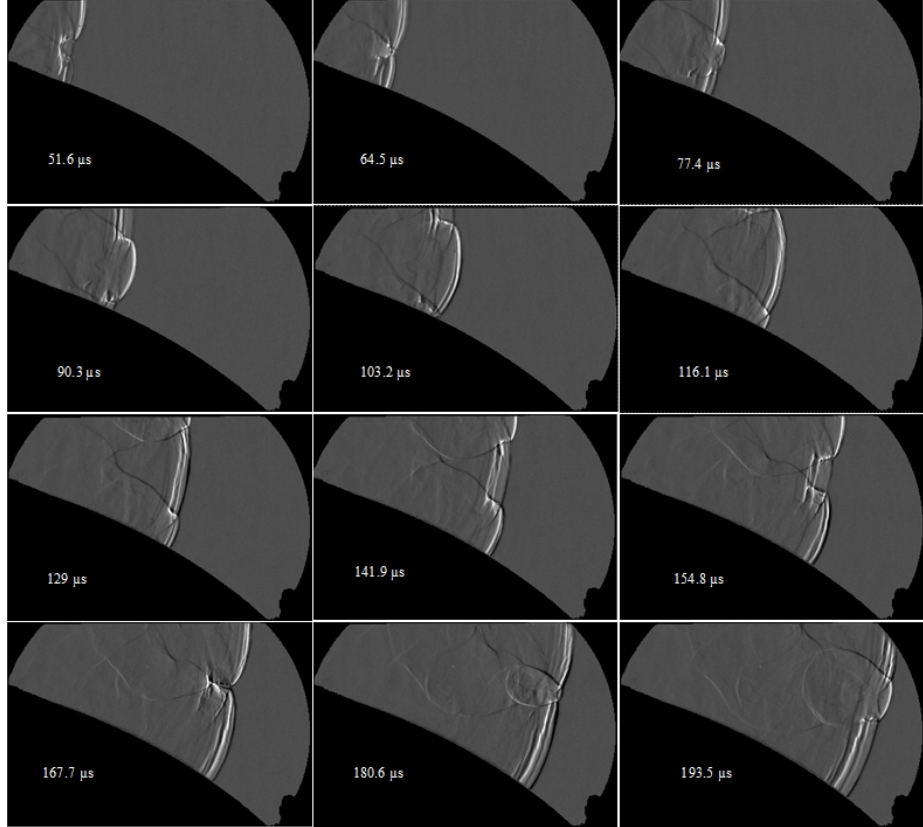


Figure 11: Schlieren photographs illustrating detonation evolution along the small ramp in the mixture of $2\text{H}_2/\text{O}_2/4.5\text{Ar}$ at the initial pressure of 11.2 kPa.

wall, which can be seen from the frames of $90.3\text{ }\mu\text{s}$ through $116.1\text{ }\mu\text{s}$ in Fig.12. This behavior can be better observed in Fig.13, showing the transition process between the non-reactive and reactive transverse waves in near-limit detonations in the mixture of $2\text{H}_2/\text{O}_2/7.0\text{Ar}$. The initially reactive transverse wave decayed gradually and transitioned to a non-reactive transverse wave, which could be seen from the frames of $64.5\text{ }\mu\text{s}$ through $141.9\text{ }\mu\text{s}$ (Fig.13). After the reflection of the non-reactive transverse wave from the bottom curved wall, considerable unreacted gases were pinched off as pockets, e.g., see frames of $154.8\text{ }\mu\text{s}$ and $167.7\text{ }\mu\text{s}$. The reflected transverse wave again became reactive and rapidly transformed to a strong transverse detonation burning all of the unreacted gases behind the leading shock. After the generation of the transverse detonation, unreacted gas pockets were no longer produced. These observations confirm Subbotin's finding of both reactive and non-reactive transverse waves existing in marginal detonations [25] and the mechanism of forming unreacted gas pockets due to inert transverse waves [25, 26, 28, 29].

Quantitatively, relationships between the mean propagation speeds and initial pressures are shown in Fig.14 for detonations in all the mixtures except $2\text{H}_2/\text{O}_2/2\text{Ar}$, along the two ramps. As the argon dilution increases, detonations of the same initial conditions propagate with a larger velocity deficit, and the critical pressure p_c also increases. This can be interpreted in terms of the

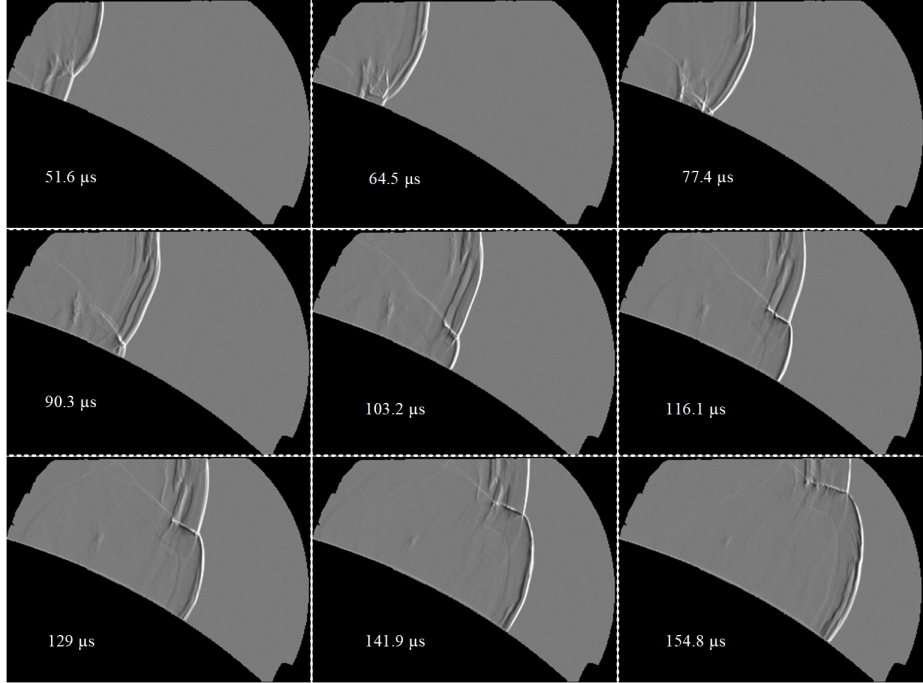


Figure 12: Schlieren photographs illustrating detonation evolution along the small ramp in the mixture of $2\text{H}_2/\text{O}_2/3\text{Ar}$ at the initial pressure of 8.8 kPa.

gas sensitivity varying with the increase in dilutions of argon. Mixtures with higher argon dilutions are the ones with reduced reaction rates and chemical energy release rates, thus giving rise to larger velocity deficits and limiting pressures. Near the limit, the measured velocity deficits can reach 20% \sim 25% of the CJ value, as is consistent with that of $2\text{H}_2/\text{O}_2/2\text{Ar}$.

4. Discussion

4.1. The experimental $D(\kappa)$ curves

The total mass divergence rate experienced by detonations propagating along ramps in this study includes two parts, the one due to the physical area divergence of the exponentially diverging channel and the other due to divergence of the flow rendered by the boundary layer growth on the channel walls. The effective lateral flow divergence rate can thus be expressed as:

$$K_{eff} = \underbrace{\frac{1}{A} \frac{dA}{dx}}_K + \phi_{BL} \quad (1)$$

where ϕ_{BL} represents the contribution of the boundary layer losses. Instead of modelling the equivalent mass divergence rate ϕ_{BL} of boundary layers, Radulescu and Borzou [22] directly evaluated this loss rate from experiments by analytically comparing the experimental data of two ramps with two underlying assumptions: (1) detonations propagating inside the exponentially

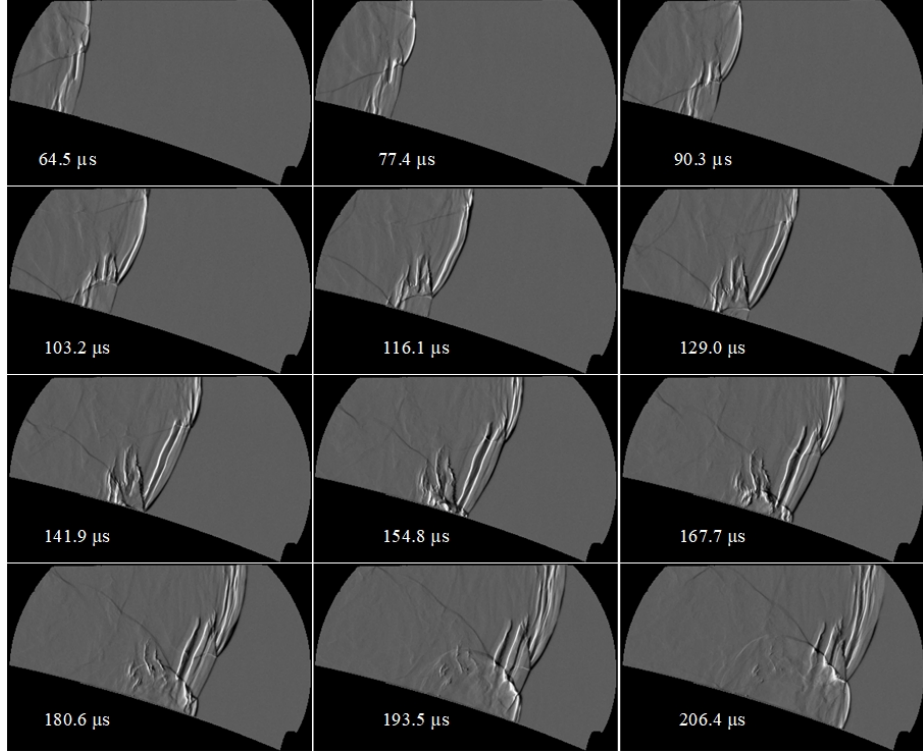


Figure 13: Schlieren photographs illustrating detonation evolution along the large ramp in the mixture of $2\text{H}_2/\text{O}_2/7\text{Ar}$ at the initial pressure of 13.8 kPa.

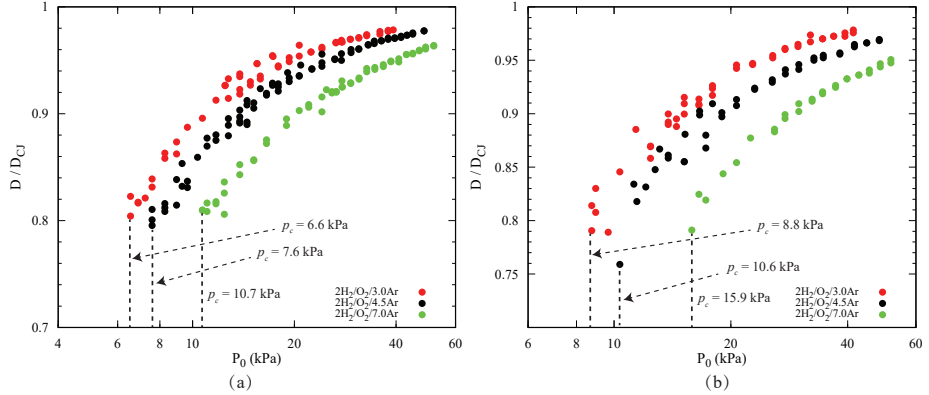


Figure 14: Normalized average speeds of (a) along the large ramp and (b) along the small ramp with respect to initial pressures for different mixtures.

diverging channel of different expansion ratios have the same constant ϕ_{BL} since the channel's dimension of the width is unchanged; (2) for the same mixture, it has a unique relation between the velocity deficits and its losses. As a result, the effective rate of total mass divergence can

be calibrated by collapsing together the experimental $D(\kappa)$ curves of detonations in the large and small ramp experiments, and then the loss rate ϕ_{BL} due to boundary layers can be derived [22]. Figure 15 shows the experimentally obtained $D(\kappa)$ curves, characterizing the relationships between the detonation velocity (normalized by the ideal CJ speed) and the lateral mass divergence, for all the mixtures involved in this study. Note that the abscissa is the non-dimensional loss obtained by multiplying the mass divergence rate with the ZND induction zone length Δ_i , which is taken as the distance between the CJ detonation front and the location of its peak thermicity. It was calculated by using the Shock and Detonation Toolbox (SDToolbox) [38] under Cantera's framework [39] with the San Diego chemical reaction mechanism (Williams 2014) [40]. This normalization method is the same as that adopted by Radulescu and Borzou [22]. In Fig.15, the graph in the right column is the collapsed $D/D_{CJ} - K_{eff}\Delta_i$ correlation, after calibrating the effective mass divergence rate K_{eff} from the $D/D_{CJ} - K\Delta_i$ curve in the corresponding left graph, by including the boundary layer effects. In the work of Radulescu and Borzou [22], the same unique value of $\phi_{BL} = 5.5 \text{ m}^{-1}$ was found to permit collapsing all data of two ramps in both mixtures of $2\text{C}_2\text{H}_2/5\text{O}_2/21\text{Ar}$ and $\text{C}_3\text{H}_8/5\text{O}_2$. However, the present study found that ϕ_{BL} can be varied for different mixtures, with 5.5 m^{-1} for $2\text{H}_2/\text{O}_2/2.0\text{Ar}$ and $2\text{H}_2/\text{O}_2/3.0\text{Ar}$, while 4.5 m^{-1} and 3.5 m^{-1} for $2\text{H}_2/\text{O}_2/4.5\text{Ar}$ and $2\text{H}_2/\text{O}_2/7.0\text{Ar}$, respectively.

4.2. Comparisons with the generalized ZND Model

4.2.1. The generalized ZND model

The governing equations for the steady, inviscid, reacting, quasi-1D flow behind the leading shock front of a detonation wave can be expressed under the frame of reference attached to the shock front as the following system of ordinary differential equations (ODEs) :

$$\frac{d}{dx'} (\rho u A_{tot}) = 0 \quad (2)$$

$$\rho u \frac{du}{dx'} + \frac{dp}{dx'} = 0 \quad (3)$$

$$\frac{d}{dx'} \left(h + \frac{1}{2} u^2 \right) = 0 \quad (4)$$

$$u \frac{dy_i}{dx'} = \frac{W_i \dot{\omega}_i}{\rho} \quad (i = 1, \dots, N_s) \quad (5)$$

where ρ , u , A_{tot} , p , h , y_i , W_i , $\dot{\omega}_i$, and N_s are the mixture density, particle velocity, total cross-sectional area, pressure, enthalpy, species mass fraction, molecular weight, molar production rate of species i , and the total number of species. x' is the distance from the shock front under the shock-attached reference. According to Fay's theory on boundary layer mechanism, its effect can be modeled by inviscid flow in a streamtube with a negative displacement of the boundary layer [4]. For the present experimental configuration, the total cross-sectional area of the exponentially diverging channel at any point o is given by $A_{tot} = H_o * (w + 2\delta^*)$. Here H_o is the channel height at point o, w is the channel width of 19 mm, and δ^* is the boundary layer negative displacement thickness induced on each side (front and back). Since the height H_o is large compared to the channel width, the boundary layer effects on the top and bottom curved wall can be reasonably neglected. The rate of total mass divergence can thus be expressed as

$$\frac{1}{A_{tot}} \frac{dA_{tot}}{dx'} = \frac{d(\ln A_{tot})}{dx'} = \frac{1}{H_o} \frac{dH_o}{dx'} + \frac{2}{(w + 2\delta^*)} \frac{d\delta^*}{dx'} \quad (6)$$

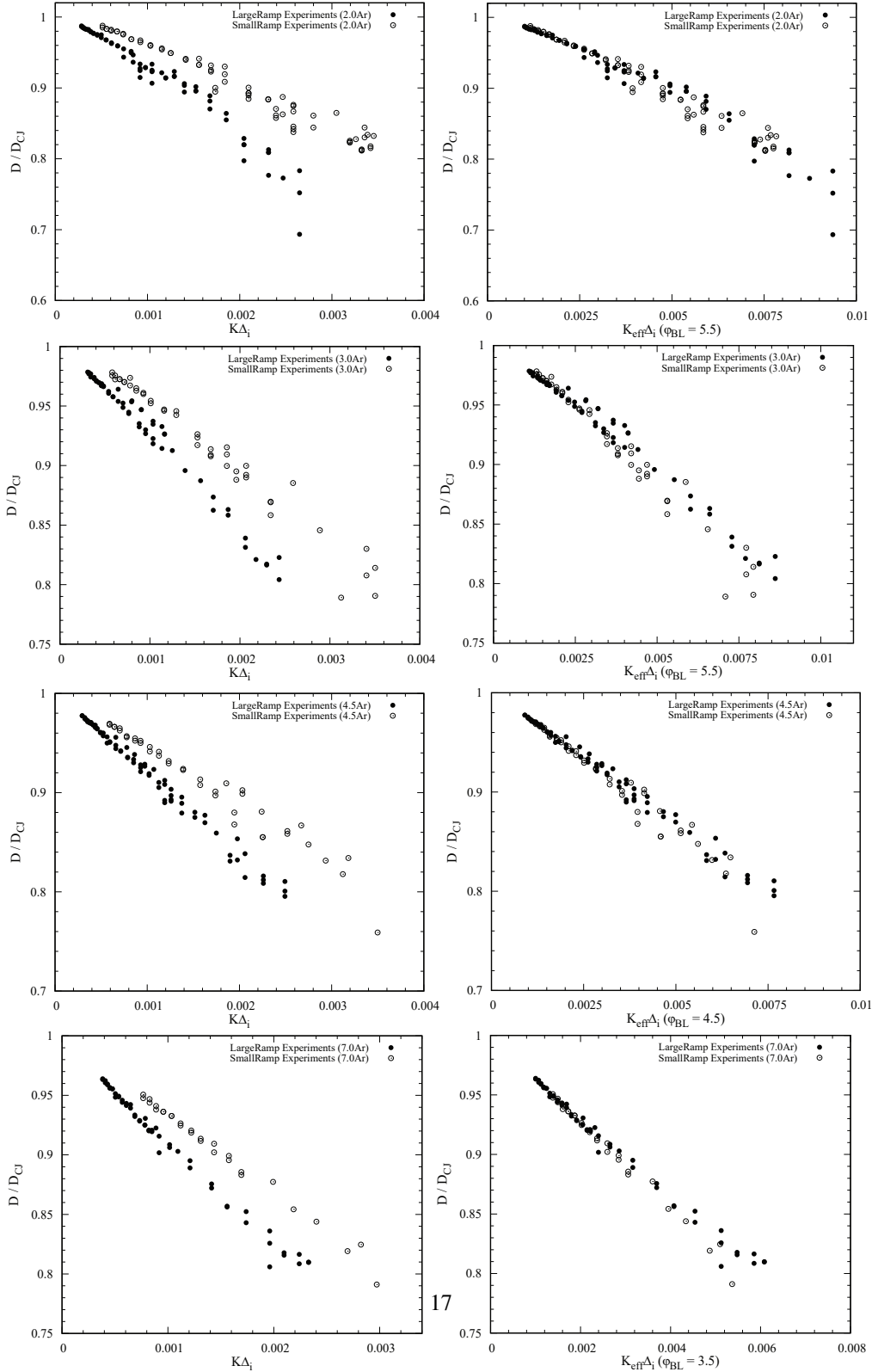


Figure 15: Experimentally obtained characteristic relationships between the detonation velocity and the lateral mass divergence, non-dimensionalized by the ZND induction zone length (Δ_i) for all the mixtures. K is the exponential area divergence rate of the channel's cross section, while K_{eff} is the total mass divergence rate by including both the cross-sectional area divergence and the boundary layer induced mass divergence.

where the first term on the right hand side is related with the rate of physical area change of the diverging channel under the lab frame of reference, and can be evaluated by the following relation [1]:

$$\frac{1}{H_o} \frac{dH_o}{dx'} = \left(\frac{D_s - u}{u} \right) \frac{d(\ln A(x))}{dx} = \left(\frac{D_s - u}{u} \right) K \quad (7)$$

where D_s is the detonation wave speed and K is the aforementioned area divergence rate of ramps. While for the second term on the right hand side in Eq.(6), it depends on the displacement thickness δ^* of the boundary layer. In Fay's work [4], he adopted the Gooderum's empirical turbulent boundary layer thickness relation [41] as the displacement thickness behind the detonation wave. The relation is given by

$$\delta^* = 0.22 (x')^{0.8} \left(\frac{\mu}{\rho_0 D_s} \right)^{0.2} \quad (8)$$

where μ and ρ_0 are the post-shock state viscosity and the initial density, respectively. This turbulent boundary layer displacement thickness relation has then been applied in a large number of subsequent works investigating detonation velocity deficits [5, 6, 9, 11–15]. In the present study, this relation is also adopted as one approach for evaluating the boundary layer induced mass divergence rate.

For the convenience of computation, the above set of equations (2)-(5) can be further simplified after mathematical manipulations [42]:

$$\frac{dp}{dt} = -\rho u^2 \frac{\dot{\sigma}_{re} - \dot{\sigma}_A}{\eta} \quad (9)$$

$$\frac{d\rho}{dt} = -\rho \frac{\dot{\sigma}_{re} - M^2 \dot{\sigma}_A}{\eta} \quad (10)$$

$$\frac{du}{dt} = u \frac{\dot{\sigma}_{re} - \dot{\sigma}_A}{\eta} \quad (11)$$

$$\frac{dy_i}{dt} = \frac{W_i \dot{\omega}_i}{\rho} \quad (i = 1, \dots, N_s) \quad (12)$$

$$\frac{dx'}{dt} = u \quad (13)$$

with

$$\eta = 1 - M^2, \quad \dot{\sigma}_{re} = \sum_{i=1}^{N_s} \left(\frac{W_i}{W} - \frac{h_i}{c_p T} \right) \frac{dy_i}{dt}, \quad \dot{\sigma}_A = \frac{u}{A_{tot}} \frac{dA_{tot}}{dx'} \quad (14)$$

where $\dot{\sigma}_{re}$ is the thermicity of ideal gases, while $\dot{\sigma}_A$ is the rate of lateral strain. M , h_i , and c_p are the local mach number, specific enthalpy of species i , and mixture specific heat at constant pressure. Here the lateral strain rate $\dot{\sigma}_A$ was evaluated by adopting two different approaches, detailed as follows, for modelling the equivalent mass divergence rate due to boundary layers.
(1) The boundary layer induced mass divergence rate is a function of the distance behind the leading shock, using the turbulent boundary layer displacement thickness relation of Eq.(8). Thus,

the lateral strain rate $\dot{\sigma}_A$ is

$$\dot{\sigma}_A = (D_s - u) K + u \left(\frac{0.352}{w + 2\delta^*} \right) \left(\frac{\mu}{\rho_0 D_s} \right)^{0.2} \left(\frac{1}{x'} \right)^{0.2} \quad (15)$$

(2) The boundary layer induced mass divergence rate is assumed constant, i.e., ϕ_{BL} , which has been directly obtained from experiments. The corresponding expression for $\dot{\sigma}_A$ becomes

$$\dot{\sigma}_A = (D_s - u) K_{eff} \quad (16)$$

For the detonation wave, the flow behind the leading shock starts from being subsonic and then accelerates towards the sonic condition due to the positive energy release of $\dot{\sigma}_{re}$. On the other hand, the strain rate of $\dot{\sigma}_A$ by the lateral flow divergence plays the opposite effect of decelerating this flow. As the flow may eventually become supersonic, a singular behavior would appear in Eqs.(9)-(11). The local balance of these two competing effects, however, can effectively prevent this singular phenomenon by mathematically letting $\dot{\sigma}_{re} = \dot{\sigma}_A$ happen at the same point for $u = c$ ($M = 1$). As a result, this so-called generalized CJ condition is satisfied with the steady reaction zone solution smoothly passing through the sonic point [42]. With this criterion, the simplified system of governing equations was numerically solved by a developed custom Python code [22] working under the framework of SDToolbox and Cantera. The San Diego chemical reaction mechanism (Williams 2014) was applied for describing the realistic chemical kinetics.

To start with, the theoretical dependence between the detonation speed and its initial pressure for each mixture was calculated. Figure 16 shows the comparison of the experimentally measured mean propagation speeds with the generalized ZND model predictions for all the presently investigated mixtures, under varied initial pressures. It can be clearly seen that Fay's model generally overpredicts the propagation velocity with respect to the corresponding experimental value, implying its underprediction of the boundary layer induced mass divergence. A possible reason for these departures can be attributed to the inappropriate assumption of turbulent boundary layer behind the detonation wave in Fay's work [4]. We estimated the Reynolds number $Re = (\rho_s u_s / \mu_s) x_H$, as shown in Fig.17, for H₂/O₂/Ar detonations in large ramp experiments. Note that ρ_s , u_s , and μ_s are the post-shock parameters, i.e., density, particle velocity (under the lab frame reference), and viscosity, while x_H is taken as the characteristic hydrodynamic thickness between the leading shock and the CJ sonic surface. The results from Fig.17 indicate that the boundary layer behind H₂/O₂/Ar detonations is probably laminar, since the Reynolds number is smaller than the critical one of $Re_c \approx 5.0 \times 10^5$. This finding concurs with the previous conclusions of Liu et al. [43] and Damazo et al. [44] that the boundary layer behind stoichiometric H₂/O₂ detonations is laminar. Therefore, Fay's turbulent boundary layer displacement thickness relation for evaluating the boundary layer induced mass divergence is questionable, and moreover, the present experiments can potentially act as a good framework for validating these relations. Interestingly, Fay's model surprisingly appears to capture the near-limit detonation dynamics quite well, including both the limit pressures and velocity deficits. The reason for this agreement is not clear and we interpret it as coincidence.

On the other hand, the experiments are found in excellent agreement with the predictions, made with the constant boundary layer induced mass divergence rate of ϕ_{BL} directly evaluated from experiments, for detonations with small and moderate velocity deficits well above the limit. While for detonations with large velocity deficits near the limit, these predictions break down. Real detonations can propagate at lower initial pressures, where the steady ZND model predicts

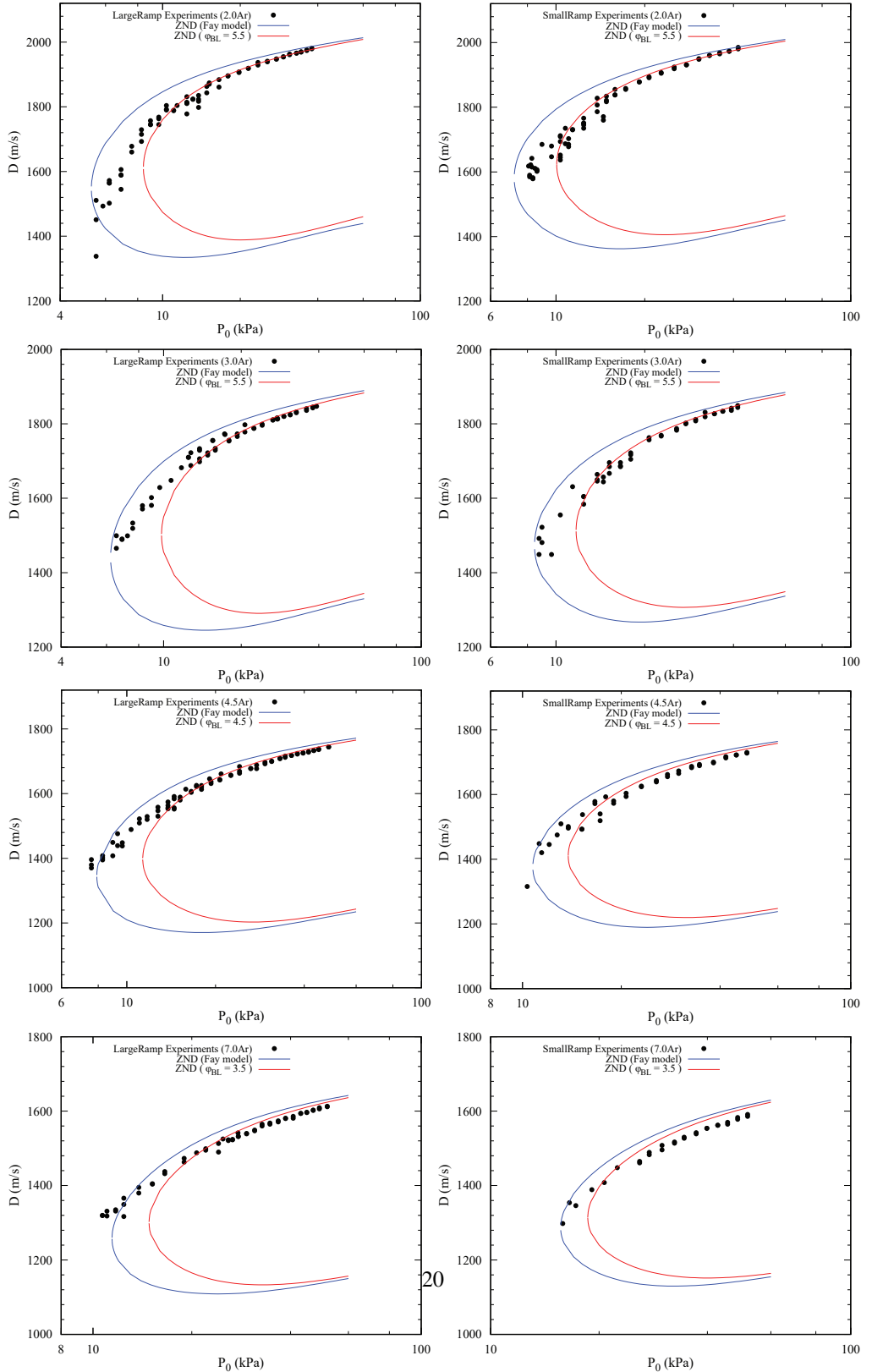


Figure 16: Comparisons of the experimentally obtained average speeds with the generalized ZND model predictions for various mixtures; the red line adopts the experimentally obtained constant divergence rate of ϕ_{BL} due to the boundary layer for the ZND model prediction, while the blue line is the prediction made with Fay's model.

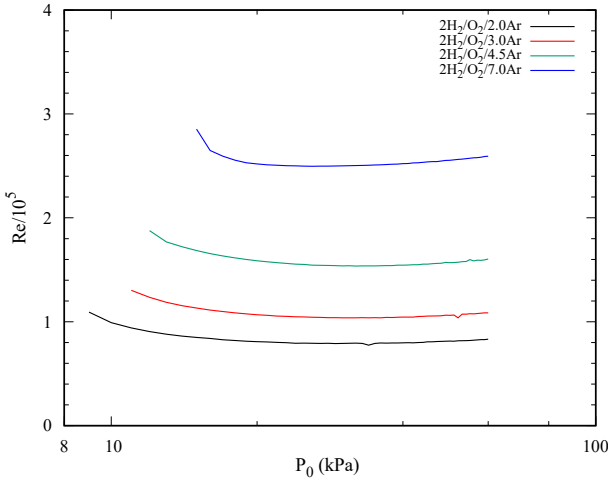


Figure 17: Reynolds number $Re = (\rho_s u_s / \mu_s) x_H$ for $H_2/O_2/Ar$ detonations with the same lateral mass divergence rate as those in large ramp experiments under varied initial pressures.

failure. The first reason for this discrepancy near the limit can be attributed to the possible promotion mechanism of strong reactive transverse waves, especially the transverse detonations, which help extend the propagation limits to lower pressures than that predicted by the generalized ZND model neglecting cellular structures. Secondly, the assumption of a constant global curvature for the leading shock front, well above the limit, is not applicable to detonations near the limit, as can be concluded from observations of the structures of detonation fronts at relatively low pressures, e.g., see Fig.3. This inappropriate application of a constant boundary layer induced mass divergence rate, for modelling detonations near the limit, thus results in failure of the theoretical predictions for the experiments.

One more explanation can be interpreted with the detonation stability in reaction zones, which has been revealed to rely on temperature fluctuations of the characteristic ignition time relative to the characteristic exothermic reaction time [18, 45, 46]. Radulescu [19] first introduced the parameter χ for characterizing the stability of detonations under different thermodynamic conditions. Detonations in mixtures of higher χ are more unstable to perturbations in the reaction zones than those with lower χ . The mathematical expression of χ is

$$\chi = \left(\frac{Ea}{RT_s} \right) \left(\frac{t_{ig}}{t_{re}} \right) \quad (17)$$

where Ea/RT_s is the usual non-dimensional activation energy, T_s is the temperature behind the leading shock, R is the universal gas constant, and t_{ig}/t_{re} is the ratio of ignition to reaction time. Figure 18 shows, for all the mixtures, the relationships of these parameters as a function of the leading shock velocity, normalized with the ideal CJ speed. Of noteworthy is that each solid circle represents one experiment, and the shock speed corresponds to the experimentally measured mean propagation velocity. One can observe that decreasing the detonation front speed by increasing the velocity deficits results in the reduced post-shock temperature, increased activation energy, and larger ratios of the ignition time relative to the reaction time, thereby enhancing the sensitivity of the reaction rates to relaxations in the reaction zones. As such, detonations tend

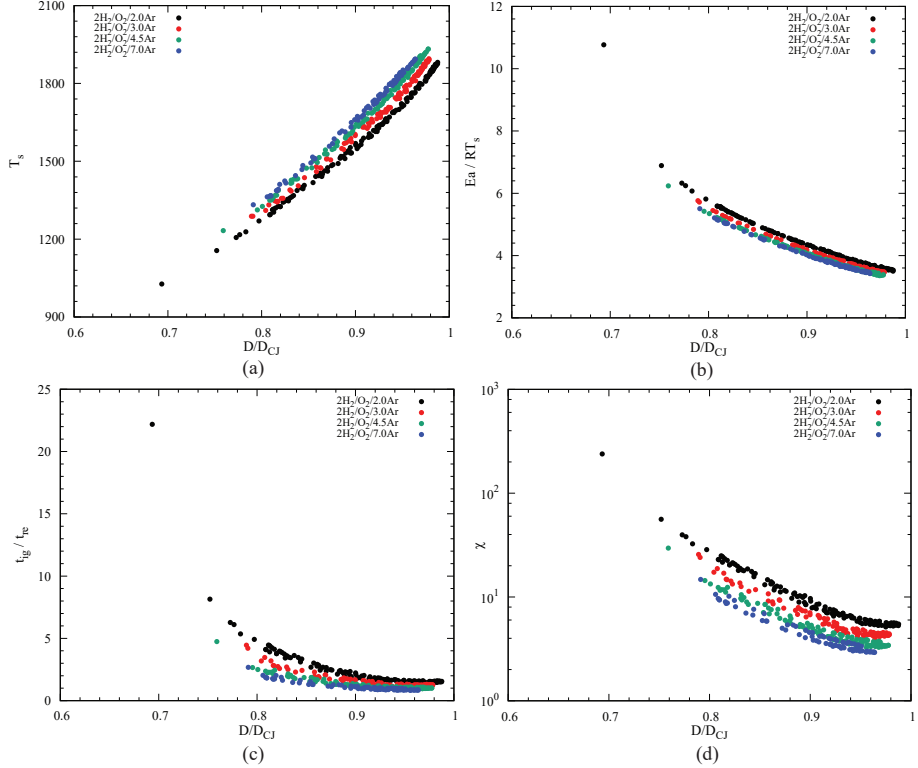


Figure 18: Parameters of (a) post-shock temperature T_s , (b) reduced activation energy $\theta = Ea/RT_s$, (c) the ratio of ignition time to reaction time, and (d) the stability parameter χ as a function of the shock speed normalized with the CJ velocity. Note that each point represents one experiment, and the shock speed corresponds to the experimentally measured mean propagation velocity. The ignition time here is defined by the time to peak thermicity, while the reaction time is defined as the inverse of the maximum thermicity, as proposed by Radulescu [19]. They were calculated with the constant volume explosion at the mean propagation speed with the San Diego chemical reaction mechanism (Williams 2014),

to become more unstable with increased χ . The considerable increment of χ , however, occurs when the velocity deficit is relatively large, especially near the limit, as can be observed from Fig.18(d). It can thus be speculated that the significantly increased instability, as a result of considerably large velocity deficits, leads to the incapability of the extended ZND model to predict detonation dynamics at relatively low initial pressures near the limit.

4.2.2. Comparison of the experimentally obtained $D/D_{CJ} - K_{eff}\Delta_i$ curves with ZND model predictions

The theoretically predicted relationship between the total lateral mass divergence rate K_{eff} and detonation speed has also been obtained. These calculations were conducted at the initial pressure of 20 kPa, which is about the midpoint of the varied initial pressures covered in experiments. Normalizing the varied divergence rate K_{eff} by the ZND induction zone length Δ_i at this pressure permits getting the theoretical $D/D_{CJ} - K_{eff}\Delta_i$ curves. Figure 19 summarizes both the $D/D_{CJ} - K_{eff}\Delta_i$ characteristic relationships, obtained from experiments and predicted from

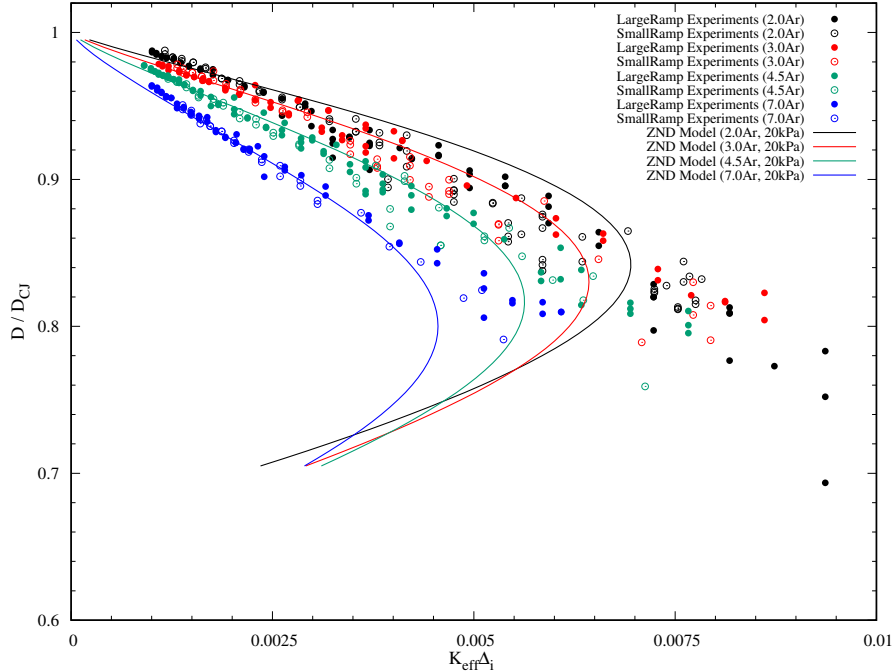


Figure 19: The $D/D_{CJ} - K_{eff}\Delta_i$ characteristic curves obtained from experiments and predicted from the quasi-1D ZND model using the San Diego chemical mechanism (Williams 2014) for different mixtures.

the quasi-1D ZND model with lateral mass divergence, respectively, for different mixtures. The experiments are found to be in excellent agreement with the extended ZND model predictions for small and moderate mass divergence, despite their breakdown for the limiting mass divergence. Detonations from experiments were able to propagate beyond the maximum mass divergence predicted by the steady ZND model, with larger velocity deficits, thus demonstrating the role of cellular structures in enhancing the detonability of gaseous detonations [47]. The experiments and ZND model predictions in Fig.19 both show that detonations with less argon dilutions can propagate with more losses. It is thus indicative of the effects of argon dilutions in reducing the detonability of $H_2/O_2/Ar$ detonations, consistent with the computations by Klein et al. [42].

4.2.3. Why can the steady 1D ZND model predict the $H_2/O_2/Ar$ cellular detonation dynamics?

The above analysis has quantitatively showed that the generalized ZND model with lateral mass divergence can excellently predict the experiments of $H_2/O_2/Ar$ cellular detonations, except for the near-limit detonation dynamics. An interesting question thus is, why can the steady 1D ZND model neglecting the transient cellular structures work?

In an attempt to clarify it, we start with the analysis of the reaction zone structure for the steady-state ZND detonations. Figure 20 shows the ZND profiles of pressure and thermicity for $H_2/O_2/Ar$ detonations under the initial pressure of 50 kPa. They were computed by utilizing the SDToolbox. Note that the pressure, distance, and time were normalized by the corresponding CJ pressure, ZND induction zone length Δ_i , and ZND induction time t_i , respectively. It is

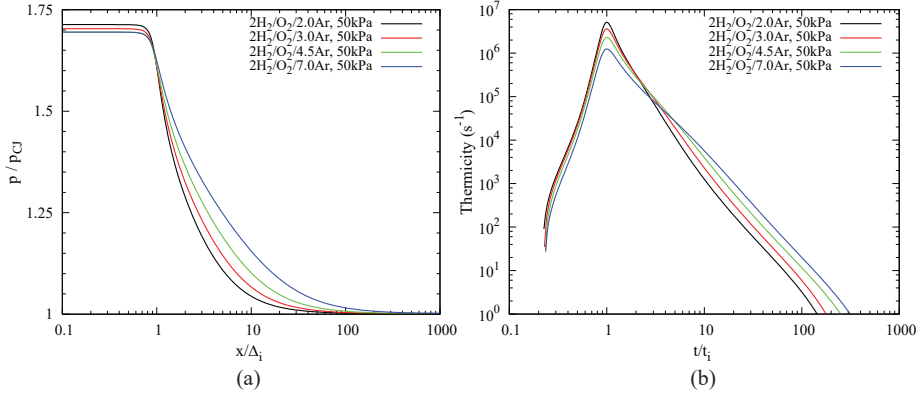


Figure 20: ZND structures of CJ detonations: (a) pressure profile as a function of the distance normalized by the induction zone length, (b) thermicity as a function of the time normalized by the induction time.

evident from Fig.20(a) that the exothermic reaction zone length (during which the pressure decreases asymptotically to the CJ pressure from the post-shock state) relative to the induction zone length is very large, in the order of 100, for H₂/O₂/Ar detonations. Correspondingly, about the same large ratio exists for the characteristic exothermic reaction time relative to the induction time (Fig.20(b)). It is the relative ratio of the induction zone to the exothermic reaction zone that determines the role of relaxations inside the induction zone in impacting the reaction zone structure. Since the induction zone is very small with short induction time, as compared to the large reaction zone, any disturbances in the short induction zone, e.g., the compression effects of the transverse waves by lifting the local pressure and temperature, can thus exert very limited influence on the global long reaction zone structure. As such, the diminished roles of transverse waves in H₂/O₂/Ar cellular detonations due to their very short induction zones give rise to quasi-1D structures, which can thus be described by the steady 1D ZND model. This can also further explain the failure of the ZND model for predicting the near-limit detonation dynamics, since detonations near the limit have the significantly increased ratio of the induction zone to reaction zone length, as can be concluded from the considerably increased induction to reaction time ratio in Fig.18(c). Therefore, the small ratio of the induction zone to reaction zone length is proposed for governing the predictability of the real H₂/O₂/Ar cellular detonation dynamics by the steady 1D ZND model.

5. Conclusion

In the present study, experiments of very regular cellular detonations, propagating inside the exponentially diverging channels with two different constant area divergence rates, were performed in mixtures of stoichiometric H₂/O₂ of varied argon dilutions. The propagation characteristics were demonstrated and analyzed in detail. The results showed that detonations, well above the limit, were uniformly curved with small-sized cellular structures of constant cell sizes, and can be reasonably assumed to propagate in quasi-steady state with a constant mean mass divergence. The experimentally measured cell sizes showed a strong dependence on the detonation velocity deficits. When the mean propagation speed dropped to $\sim 0.8D_{CJ}$, detonations started

to propagate in the mechanism of single-headed detonations, organized with a distinctive transverse detonation, with the detonation cell size larger than the ideal one in the order of $10 \sim 15$. The stabilization mechanism of single-headed detonations with saliently enlarging cells suggests a higher growth rate of the curved detonation front area than that of the intrinsic transverse instability. The Go/No-Go phenomenon has also been demonstrated for detonations near the very limit, due to its stochastic property. Also, both the reactive and non-reactive transverse waves were observed for detonations propagating at low pressures near the limit.

Quantitatively, the experimental $D/D_{CJ} - K_{eff}\Delta_i$ curves were obtained by collapsing the $D/D_{CJ} - K\Delta_i$ relationships of both the large ramp and small ramp. As a result, the equivalent mass divergence rates ϕ_{BL} due to boundary layers were directly derived. It was found that detonations of lower argon dilutions can propagate with more losses, indicating the effects of argon addition in decreasing the detonability of $H_2/O_2/Ar$ detonations. Furthermore, comparisons between the experimentally obtained average speeds and the generalized ZND model predictions were performed in terms of different initial pressures. The results showed that predictions made with the experimentally obtained flow divergence rate ϕ_{BL} can predict the experiments better than Fay model, whose questionable concept of turbulent boundary layer behind detonations was clarified by estimating the Reynolds number. The variation of velocity deficits with mass divergence was also found in excellent agreement with the predictions made with steady ZND model with lateral mass divergence, for small and moderate divergence and velocity deficits. Nevertheless, the model underpredicted the limiting mass divergence and velocity deficits for detonations near the limit, thus illustrating the effects of cellular structures in enhancing the detonability. The promotion effects by the strong reactive transverse waves or transverse detonations, the inappropriate application of the constant mass divergence assumption near the limit, and the considerably increased instability were proposed for the possible reasons for these discrepancies. Finally, the small ratio of the induction zone to reaction zone length was proposed for clarifying the excellent predictability of the real $H_2/O_2/Ar$ cellular detonation dynamics by the extended 1D ZND model with lateral mass divergence.

Acknowledgments

The authors acknowledge the financial support from the Natural Sciences and Engineering Research Council of Canada (NSERC) through the Discovery Grant "Predictability of detonation wave dynamics in gases: experiment and model development". The authors would also like to thank Jiaxin Chang, Maxime La Fleche, and Yongjia Wang for help in conducting the experiments, and thank S.M. Lau-Chapdelaine for the code for postprocessing the shadowgraph and schlieren photographs.

References

References

- [1] W. Fickett, W. C. Davis, *Detonation* (Berkeley (1979)).
- [2] J. H. S. Lee, *The Detonation Phenomenon*, Cambridge University Press, 2008. [doi:10.1017/CBO9780511754708](https://doi.org/10.1017/CBO9780511754708).
- [3] Y. B. Zeldovich, On the theory of the propagation of detonation in gaseous systems.
- [4] J. A. Fay, Two-dimensional gaseous detonations: Velocity deficit, *The Physics of Fluids* 2 (3) (1959) 283–289.
- [5] J. Dove, B. Scroggie, H. Semerjian, Velocity deficits and detonability limits of hydrogen-oxygen detonations, *Acta Astronautica* 1 (3-4) (1974) 345–359.

[6] S. B. Murray, The influence of initial and boundary conditions on gaseous detonation waves., Tech. rep., Defence Research Establishment Suffield Ralston (Alberta) (1985).

[7] G. Agafonov, S. Frolov, Computation of the detonation limits in gaseous hydrogen-containing mixtures, *Combustion, Explosion and Shock Waves* 30 (1) (1994) 91–100.

[8] K. Ishii, K. Itoh, T. Tsuboi, A study on velocity deficits of detonation waves in narrow gaps, *Proceedings of the Combustion Institute* 29 (2) (2002) 2789–2794. doi:[https://doi.org/10.1016/S1540-7489\(02\)80340-6](https://doi.org/10.1016/S1540-7489(02)80340-6) URL <http://www.sciencedirect.com/science/article/pii/S1540748902803406>

[9] J. Chao, H. Ng, J. Lee, Detonability limits in thin annular channels, *Proceedings of the Combustion Institute* 32 (2) (2009) 2349–2354.

[10] S. Kitano, M. Fukao, A. Susa, N. Tsuboi, A. Hayashi, M. Koshi, Spinning detonation and velocity deficit in small diameter tubes, *Proceedings of the combustion institute* 32 (2) (2009) 2355–2362.

[11] A. Camargo, H. D. Ng, J. Chao, J. H. Lee, Propagation of near-limit gaseous detonations in small diameter tubes, *Shock Waves* 20 (6) (2010) 499–508.

[12] K. Ishii, M. Monwar, Detonation propagation with velocity deficits in narrow channels, *Proceedings of the Combustion Institute* 33 (2) (2011) 2359–2366.

[13] B. Zhang, X. Shen, L. Pang, Y. Gao, Detonation velocity deficits of h₂/o₂/ar mixture in round tube and annular channels, *international journal of hydrogen energy* 40 (43) (2015) 15078–15087.

[14] Y. Gao, B. Zhang, H. D. Ng, J. H. Lee, An experimental investigation of detonation limits in hydrogen–oxygen–argon mixtures, *international journal of hydrogen energy* 41 (14) (2016) 6076–6083.

[15] B. Zhang, H. Liu, C. Wang, B. Yan, An experimental study on the detonability of gaseous hydrocarbon fuel/oxygen mixtures in narrow channels, *Aerospace Science and Technology* 69 (2017) 193 – 200. doi:<https://doi.org/10.1016/j.ast.2017.06.032> URL <http://www.sciencedirect.com/science/article/pii/S1270963817304029>

[16] M. I. Radulescu, J. H. Lee, The failure mechanism of gaseous detonations: experiments in porous wall tubes, *Combustion and Flame* 131 (1-2) (2002) 29–46.

[17] J. Shepherd, Detonation in gases, *Proceedings of the Combustion Institute* 32 (1) (2009) 83 – 98. doi:<https://doi.org/10.1016/j.proci.2008.08.006> URL <http://www.sciencedirect.com/science/article/pii/S1540748908001806>

[18] M. I. Radulescu, H. D. Ng, J. H. Lee, B. Varatharajan, The effect of argon dilution on the stability of acetylene/oxygen detonations, *Proceedings of the Combustion Institute* 29 (2) (2002) 2825–2831.

[19] M. I. Radulescu, The propagation and failure mechanism of gaseous detonations: experiments in porous-walled tubes, Ph.D. thesis, McGill University Libraries (2003).

[20] A. Chinnayya, A. Hadjadj, D. Ngomo, Computational study of detonation wave propagation in narrow channels, *Physics of Fluids* 25 (3) (2013) 036101.

[21] K. Mazaheri, Y. Mahmoudi, M. Sabzpooshani, M. I. Radulescu, Experimental and numerical investigation of propagation mechanism of gaseous detonations in channels with porous walls, *Combustion and Flame* 162 (6) (2015) 2638–2659.

[22] M. I. Radulescu, B. Borzou, Dynamics of detonations with a constant mean flow divergence, *Journal of Fluid Mechanics* 845 (2018) 346377. doi:[10.1017/jfm.2018.244](https://doi.org/10.1017/jfm.2018.244).

[23] G. Settles, *Schlieren and shadowgraph techniques- visualizing phenomena in transparent media(book)*, Berlin, Germany: Springer-Verlag GmbH, 2001.

[24] M. Kaneshige, J. E. Shepherd, Detonation database.

[25] V. Subbotin, Two kinds of transverse wave structures in multifront detonation, *Combustion, Explosion and Shock Waves* 11 (1) (1975) 83–88.

[26] G. J. Sharpe, Transverse waves in numerical simulations of cellular detonations, *Journal of Fluid Mechanics* 447 (2001) 3151. doi:[10.1017/S0022112001005535](https://doi.org/10.1017/S0022112001005535).

[27] F. Pintgen, C. Eckett, J. Austin, J. Shepherd, Direct observations of reaction zone structure in propagating detonations, *Combustion and Flame* 133 (3) (2003) 211 – 229. doi:[https://doi.org/10.1016/S0010-2180\(02\)00458-3](https://doi.org/10.1016/S0010-2180(02)00458-3) URL <http://www.sciencedirect.com/science/article/pii/S0010218002004583>

[28] J. M. Austin, The role of instability in gaseous detonation.

[29] V. Gamezo, A. Vasil'ev, A. Khokhlov, E. Oran, Fine cellular structures produced by marginal detonations, *Proceedings of the Combustion Institute* 28 (1) (2000) 611–617.

[30] M. Short, C. Chiquete, J. J. Quirk, Propagation of a stable gaseous detonation in a circular arc configuration, *Proceedings of the Combustion Institute* 37 (3) (2019) 3593–3600.

[31] B. MCBRIDE, S. Gordon, Computer program for calculation of complex chemical equilibrium compositions and applications.

[32] J. Loiseau, A. J. Higgins, Statistical measurement of critical tube diameter, in: 21st International Colloquium on the Dynamics of Explosions and Reactive Systems, 2007.

[33] R. Mével, Q. Xiao, M. Radulescu, Hydrogen-oxygen-argon detonation diffraction in a narrow channel, in: 26th International Colloquium on the Dynamics of Explosions and Reactive Systems, 2017.

[34] C. Engel, R. Strehlow, Transverse waves in detonations. ii-structure and spacing in h₂-o₂, c₂h₄-o₂, and ch₄-o₂ systems., AIAA journal 7 (3) (1969) 492–496.

[35] H. O. Barthel, Predicted spacings in hydrogen-oxygen-argon detonations, The Physics of Fluids 17 (8) (1974) 1547–1553.

[36] I. Moen, M. Donato, R. Knystautas, J. Lee, The influence of confinement on the propagation of detonations near the detonability limits, Symposium (International) on Combustion 18 (1) (1981) 1615 – 1622. doi:[https://doi.org/10.1016/S0082-0784\(81\)80165-8](https://doi.org/10.1016/S0082-0784(81)80165-8).

[37] J. H. Lee, A. Jesuthasan, H. D. Ng, Near limit behavior of the detonation velocity, Proceedings of the Combustion Institute 34 (2) (2013) 1957 – 1963. doi:<https://doi.org/10.1016/j.proci.2012.05.036>.

[38] S. Brown, J. Shepherd, Numerical solution methods for control volume explosions and znd structure, GALCIT Report, July.

[39] D. G. Goodwin, H. K. Moffat, R. L. Speth, Cantera: An object-oriented software toolkit for chemical kinetics, thermodynamics, and transport processes, <http://www.cantera.org>, version 2.3.0 (2017). doi:10.5281/zenodo.170284.

[40] F. A. Williams, 2014 chemical-kinetic mechanisms for combustion applications, san diego mechanism web page, mechanical and aerospace engineering (combustion research), <http://combustion.ucsd.edu>, university of California at San Diego (2014).

[41] P. B. Gooderum, An experimental study of the turbulent boundary layer on a shock-tube wall.

[42] R. Klein, J. C. Krok, J. Shepherd, Curved quasi-steady detonations: Asymptotic analysis and detailed chemical kinetics.

[43] W. Liu, I. Glass, Laminar boundary layers behind detonation waves, Proc. R. Soc. Lond. A 387 (1793) (1983) 331–349.

[44] J. Damazo, J. Odell, J. Shepherd, Boundary layer profile behind gaseous detonation as it affects reflected shock wave bifurcation, in: 42nd AIAA Fluid Dynamics Conference and Exhibit, 2012, p. 2975.

[45] J. Meyer, A. Oppenheim, Coherence theory of the strong ignition limit, Combustion and Flame 17 (1) (1971) 65–68.

[46] F. Zhang, Shock Waves Science and Technology Library, Vol. 6: Detonation Dynamics, Vol. 6, Springer Science & Business Media, 2012.

[47] M. I. Radulescu, A detonation paradox: Why inviscid detonation simulations predict the incorrect trend for the role of instability in gaseous cellular detonations?, Combustion and Flame 195 (2018) 151 – 162, special Commemorative Issue: Professor Chung King (Ed) Law 70th Birthday. doi:<https://doi.org/10.1016/j.combustflame.2018.05.002>.
URL <http://www.sciencedirect.com/science/article/pii/S0010218018301962>